Published in final edited form as:
Adv Mater. 2013 October 18; 25(39): 5632–5637. doi:10.1002/adma201301804.

Fluorinated Graphene Oxide; a New Multimodal Material for Biological Applications

Rebeca Romero-Aburto,
Department of Mechanical Engineering & Materials Science, Rice University, 6100 Main St. Houston, TX 77005 USA. Department of Translational Molecular Pathology, MD Anderson Cancer Center 7435 Fannin Street, Houston, TX 77054 USA

Dr. Tharangattu. N. Narayanan,
Department of Mechanical Engineering & Materials Science, Rice University, 6100 Main St. Houston, TX 77005 USA. CSIR-Central Electrochemical Research Institute, Karaikudi 630 006, Tamilnadu India

Dr. Yutaka Nagaoka,
Bio-Nano Electronics Research Center, Toyo University, 2100, Kujirai, Kawagoe, Saitama 350 8585, JP

Dr. Takashi Hasumura,
Bio-Nano Electronics Research Center, Toyo University, 2100, Kujirai, Kawagoe, Saitama 350 8585, JP

Trevor M. Mitcham,
Department of Imaging Physics, MD Anderson Cancer Center 1881 East Rd. Houston, TX 77054 USA

Dr. Takahiro Fukuda,
Bio-Nano Electronics Research Center, Toyo University, 2100, Kujirai, Kawagoe, Saitama 350 8585, JP

Dr. Paris J. Cox,
Department of Mechanical Engineering & Materials Science, Rice University, 6100 Main St. Houston, TX 77005 USA

Prof. Richard R. Bouchard,
Department of Imaging Physics, MD Anderson Cancer Center 1881 East Rd. Houston, TX 77054 USA

Prof. Toru Maekawa,
Bio-Nano Electronics Research Center, Toyo University, 2100, Kujirai, Kawagoe, Saitama 350 8585, JP

Prof. D. Sakthi Kumar,
Bio-Nano Electronics Research Center, Toyo University, 2100, Kujirai, Kawagoe, Saitama 350 8585, JP

Prof. Suzy V. Torti,
Department of Molecular, Microbial and Structural Biology, University of Connecticut Health Center, 263 Farmington Ave, Farmington CT06030 USA

Correspondence to: Sendurai A. Mani, smani@mdanderson.org; Pulickel M. Ajayan, ajayan@rice.edu.

Supporting Information
Supporting Information is available online from the Wiley Online Library or from the author.

Prof. Sendurai A. Mani, and
Department of Translational Molecular Pathology, MD Anderson Cancer Center 7435 Fannin Street, Houston, TX 77054 USA

Prof. Pulickel M. Ajayan
Department of Mechanical Engineering & Materials Science, Rice University, 6100 Main St. Houston, TX 77005 USA

Sendurai A. Mani: smani@mdanderson.org; Pulickel M. Ajayan: ajayan@rice.edu

Abstract

Fluorinated graphene oxide (FGO) is reported for the first time as a magnetically responsive drug carrier that can serve as a MRI and photoacoustic contrast agent, under pre-clinical settings, as well as a photothermal therapy Its hydrophilic nature facilitates biocompatibility. FGO as a broad wavelength absorber, with high charge transfer and strong nonlinear scattering is optimal for NIR laser-induced hyperthermia.

Keywords

multifunctional graphene; MRI; photoacoustic; photothermal therapy; drug delivery

Recent advancement in drug delivery using nanotechnology achieves enhanced circulation half-life and controllable drug release. Some of the newer drug delivery approaches utilize a combination of materials to achieve multimodality, such as, one material serves as a biocompatible photo-thermal Near Infra-Red (NIR) laser inducible agent that can be loaded with drug, while the second material in the system might work as a clinical contrast agent for MRI or ultrasound. However, few single materials with such multimodal capabilities are reported.[1,2]

Among the known multimodal composites, the most widely used consists of gold nanoparticles (AuNPs) that are color tunable from the visible to NIR region. In addition to inducing hyperthermia and/or drug release due to their plasmonic properties.[3–7] Carbon materials, such as carbon nanotubes (CNTs), graphene and specifically graphene oxide (GO) have been studied for biological applications including drug delivery, and biosensing.[8–22] The presence of diverse functional groups in GO allow chemical incorporation of targeting agents, or therapeutically relevant molecules,[23–26] such as physical adsorption via π-π stacking interactions.[27] Due to the excellent charge transfer properties of CNT's and GO, they have been used to achieve hyperthermia.[28] However, for MRI, either gold nanoparticles or carbon nanomaterials are not sufficient to perform as contrast agents. Therefore, super paramagnetic iron oxide nanoparticles (SPION) have been assorted with approaches containing AuNPs,[29,30] CNT's or GO[31–34] to create composites that serve as MRI contrast agents. MRI is desirable due to the ability to resolve physiological and anatomical details without utilizing ionizing radiation. Until now, there are no reports that show carbon materials conferring MRI contrast without the incorporation of magnetic nanoparticles.

In addition to the above mentioned agents, fluorinated (^{19}F) contrast agents are highly desirable due to the scarce distribution of fluorine in the human body and their ability to be detected by magnetic resonance imaging (MRI)[35] as well as ultrasound.[36] Moreover, several fluorine (F) containing compounds have also been widely used in medicine as therapeutic drugs.[37] At present, to achieve combined MRI and ultrasonography, perfluorocarbon microbubbles (PFCMB), the state of the art in contrast agents for ultrasonography,[38,39] have been combined with SPIONs to confer MRI detection.[40]

Recently, we developed a novel method to synthesize large quantities of fluorinated graphene oxide (FGO), and extensive characterization of the material has been reported.[41,42] In this manuscript we demonstrate FGO as a multimodal material for biological applications. In fact, we found FGO being the first carbon material to confer MRI without the addition of magnetic nanoparticles. Similar to GO, synthesized FGO has several functional groups in its lattice thus allowing for the same diverse chemical functionalization and loading capabilities as GO. Moreover, FGO like other carbon materials is proven to absorb NIR-laser energy and efficiently transform it into heat. MRI studies conducted on FGO phantoms were seen to exhibit higher negative contrast than GO phantoms. Under a rotational magnetic field FGO is responsive to a 12mT field. Ultrasound showed FGO to be hyperechoic in comparison to anechoic agar. In summary, we report FGO as a single multimodal material capable of serving as a contrast agent for MRI, ultrasound and photoacoustic imaging. Furthermore, FGO serves as a targetable drug carrier and NIR-laser inducible hyperthermic material that can ablate thermo-sensitive cancer cells.

Although GO has been extensively reported for its biomedical applications, including *in-vivo* strategies, recent reports suggest that various negatively charged functional groups present in GO can induce thromboembolism (aggregation of platelets in blood).[43] Singh *et al.* reported that surface charge of graphene could play a key role in the interaction between graphene and platelets. Furthermore, they demonstrated that amine functionalized graphene is a better candidate for biomedical applications due to its positive surface charge, hence avoiding thrombotic and hemolytic predisposition.[44] This can be due to the $–NH_3^+$ formation of $–NH_2$ with the adjacent proton in solution or at the interface with biomolecules. Fluorine also modifies the electronic properties of graphene by reducing the charge in the conducting π orbitals.[45] Hence low level inhomogeneous doping of highly electronegative F can induce partial positive surfaces on graphene. However, complete spatial charge separation is unlikely due to the high charge mobility of graphene. The hydrophobic centers in FGO (or fluorinated graphene in the case of reduced FGO) may also act as energetic barriers between platelet membrane and FGO, hence preventing thromboembolism. Moreover, F doping can greatly increase the lipophilicity of drug carrier/molecule, an important consideration when designing drug delivery systems/molecules that are designed to be active *in vivo*.[46]

Similar to oxidizing chemical exfoliation of the graphite basal plane, which introduces functional groups generating GO,[47,48] we exfoliated fluorinated graphite and produced FGO. The resulting FGO is composed of alkyl fluorides, epoxy, carbonyl, carboxylic and hydroxyl groups covalently bonded to the carbon lattice.[41] Most importantly, addition of these oxygen functionalities makes FGO hydrophilic.[41] Further characterization of FGO suggested a characteristic sheet like morphology evidenced by Atomic Force Microscopy (AFM) (Figure 1A, Figure S1A), Transmission Electron Microscopy (TEM) (Figure 1B) and Scanning Electron Microscopy (SEM) (Figure S1B), corresponding to traditional 2D graphene material. The AFM results suggest that the thickness of a typical FGO sheet is < 1 nm, indicating the presence of 1–2 layered FGO. The lateral width seems to be around 1 μm and it correlates with the TEM data.

Incubation of FGO with human breast cancer cell line MCF-7 did not show any cytotoxicity even after 3 days with a concentration of up to 576 $\mu g\ mL^{-1}$ (Figure 1C). This clearly shows that FGO is potentially non-toxic similar to the previous finding for GO using various other cell lines, predominantly due to the availability of various oxygen containing functional groups.[49–51]

Functional groups in FGO permit π-π stacking interactions or covalent bonding of therapeutic and targeting agents. To load chemotherapeutics, such as Doxorubicin (DOX) by

means of π-π stacking interactions, DOX was mixed with FGO-COOH (1:1 v/v) overnight at 4 °C and after centrifugal washes to separate the unbound drug UV-Vis spectroscopic analysis was performed to identify the interaction between DOX molecule and FGO. DOX (~480nm)[52] as well as FGO (~230nm)[24] displayed their characteristic peaks in UV-Vis spectra consistent with earlier reports. Besides, an additional peak is observed at 490nm in FGO loaded with doxorubicin (FGO-DOX) indicative of DOX interaction with FGO through non-covalent attractive forces (Figure 1D).[53] Moreover, using photoluminescence, we found a reduction in DOX fluorescence due to quenching mediated by the interaction with FGO (Figure 1E). Collectively, these data suggest that FGO could be used to non-covalently load therapeutic agents.

The presence of fluorine in FGO's basal plane can (dipolar C-F bonds) introduce paramagnetic centers. In fact, using SQUID characterization at 300K, we found a linear dependency to the magnetic field, proving that FGO exhibits paramagnetic behavior (Figure 2A). Since FGO is responsive to a 5T magnetic field (Figure 2A), we scanned MRI phantoms on a 4.7 T Biospec System (Figure 2B) to determine if FGO could serve as a MRI contrast agent. Due to structural similarities between FGO and GO, we compared them for their ability to serve as MRI contrast agents. As predicted, FGO exhibits contrast in T2 mode (Figure 2B) while GO did not. We used relaxed water (0.5 mg mL^{-1} of magnevist) as a positive control. This suggest that the paramagnetic behavior in FGO is attributed to the presence of fluorine (C-F bonds), therefore in biological environments, materials like FGO will have higher signal to noise ratio because of the scarce distribution of ^{19}F as opposed to protons (^{1}H) in the body. To further test FGO's magnetic response, rotational magnetic field experiments were performed under an optical microscope (details are provided in the supporting information) and snapshots taken from the recorded video fragments (Figure 2C). The results show that FGO can be magnetically triggered, even with a small system of electromagnets having a magnetic field of 12mT, which is further evident in the video (Supplemental video 1). This emphasizes the dramatic change in physical properties of GO due to the presence of small amounts of F in its lattice.

Earlier experiments conducted to compare diagnostic techniques to detect breast cancer revealed that the combination of MRI and ultrasound yields the best results.[54] Since FGO has been proven to confer MRI contrast; we also investigated its ability as an ultrasound detection agent. FGO was imaged at a 40-MHz center frequency and generated appreciable acoustic backscattering, as demonstrated by the hyperechoic regions in Figure 3A. As expected, pure agar without added scatterers, which served as the negative control, presented as entirely anechoic (Figure 3B), while the positive control PFCMB, generated a strong backscatter signal (Figure 3C). Most importantly, we observed a strong backscatter signal using FGO's (291.2 μg mL^{-1}), which is qualitatively significantly stronger than pure agar. These results suggest that FGO could be used as an ultrasound contrast agent. The spectroscopic imaging of FGO and GO generated similar photoacoustic signal spectrum (Figure 3F), which peaked at 720 nm. When evaluated at a preclinical frequency (21MHz), FGO was well visualized with PA imaging (Figure 3E), while it was poorly visualized when relying on ultrasound alone (Figure 3D). The inability of FGO to provide a better ultrasound signal is probably due to the reduction in frequency from 40 to 21MHz.

The value of a drug carrier like FGO's can be maximized if this material can be photo heated, due to its applicability as a cancer photothermal therapy.[55–57] Cell culture conditions were used to investigate the hyperthermic ability of FGO when irradiated with an 800nm NIR-laser (Chameleon Ultra, Coherent Inc.), with a power of 1.6 W (details are given in experimental section). Temperature of the tissue culture sample containing FGO increased to 62.3°C within one minute of irradiation, relative to control culture media without FGO, which remained at ≤25.0°C following irradiation (Figure 4A). To test,

whether NIR-laser energy transformed to heat by FGO could induce cell death, we exposed glioma cancer cells (GI-1), in the presence and absence of FGO and irradiated them with NIR-laser. The cells containing FGO exhibited significant cell death evidenced by an increase in staining for necrosis related to propidium iodide as well as apoptosis related annexin-V FITC (bottom panel of Figure 4B) compared to the cells without FGO (top panel of Figure 4B). Collectively, these findings indicate that FGO could be used to increase the local temperature and induce cell death. Since we observed that heat dissipation occurs within 1 min after laser irradiation and there are no indicatives of apoptosis or necrosis outside the irradiation radial zone; suggesting that FGO can be used to specifically ablate cancer tissues without damaging nearby healthy tissues (top panel of Figure 4B).[58]

The results presented here indicate that FGO is a theranostic material that exhibits multimodal imaging, including MRI, ultrasound and photoacoustic. Furthermore, drug loading as well as the ability to induce hyperthermia via NIR-laser can be achieved with FGO. A strong backscattering signal from FGO was observed under ultrasonography, opening the possibility for a second imaging modality. One limitation of using FGO in ultrasonography is the requirement of micron-size scatterers, which would tend to limit the agent to the vasculature. Nevertheless, for photoacoustic imaging, the scatterer's size is no longer a requirement. Therefore, FGO's ability to absorb NIR-laser energy makes it suitable for photoacoustic imaging, thus enabling micro or nanoscopic FGO to be employed in strategies that seek crossing the vasculature. Additionally, the ability to convert the absorbed NIR-laser energy into heat to increase the local temperature could serves as an excellent therapeutic agent against cancer cells that are sensitive to higher temperatures. The induced hyperthermia can potentially be employed as a release mechanism for therapeutic agents that have been conjugated to FGO. Moreover, attaching a targeting entity to the loaded nano-FGO will facilitate selective targeting to the tumor environment or tissue of interest.

In conclusion, we found that FGO is a novel carbon material with clinically translatable multimodal capabilities. These include, the ability to serve as MRI, ultrasound and photoacoustic contrast agents, as well as having the potential to load hydrophobic therapeutic agents to the hydrophilic FGO basal plane. Notably, it can serve as a photothermal ablation agent when irradiated with a NIR-laser. Future refinement and differential size selection of FGO as well as testing targeted nano-FGO for its synergistic hyperthermia and drug release *in vitro* and *in vivo* will make FGO a more attractive agent for various diseases including cancer.

Experimental section

I) Preparation of Fluorinated Graphene Oxide (FGO)

Briefly, graphite fluorinated polymer (2g) (Alfa Aesar, Ward Hill, MA, USA) were exfoliated using the modified Hummer's method. Detailed synthesis protocol has been reported elsewhere.[41,47]

II) Particle shape and morphology

Drop casted powder FGO morphology was obtained by Field Emission SEM (FEI Quanta 400) with a working voltage of 10 kV. JEOL 2100 Field Emission Gun Transmission Electron Microscope is used to image the drop casted FGO solution on a copper holey carbon grid with a working voltage of 200 kV. AFM images were obtained at ambient conditions using Asylum Research model MFP-3D.

III) Cytotoxicity studies

Cells were cultured and maintained in DMEM medium (Invitrogen) containing fetal bovine serum (FBS, 10%) and penicillin/streptomycin (P/S, 1%) antibiotics. The same medium was used as a solvent for the serial dilutions of FGO. Human breast cancer cell line MCF-7, were seeded in a 96 well plate (1×10^3 cells/well; 100μL/well) and incubated for 1 day to allow cell adhesion to the plate. On the following day, different concentrations of FGO (50μL) were added to each well giving a final concentration of (72, 144, 287, 575 μg mL^{-1}) respectively and incubated for 24, 48 and 72 hrs. At the end of the study, 3-(4,5-dimethyl-2-thiazolyl)-2, 5-diphenyltetrazolium bromide (MTT, 5mg mL^{-1}, 50μL/well) was added and incubated for 4.5 h. After MTT removal, dimethyl sulfoxide (DMSO, 200 μL/well) was added; the reagent was left for 10 min before optical density of solubilized formazan salts was assessed at 570nm in a μQuantplate reader (Bio-Tek Instruments Inc.)

IV) Drug loading characterization

Room temperature absorbance measurements were carried out in a Beckman Coulter DU730 spectrophotometer from 200 to 700nm. Photoluminescence experiments were done in a Hitachi F-4500 fluorescence spectrometer with 150W Xe lamp as a light source (λ_{ex}= 300nm) and a step of 0.2nm.

V) Magnetization measurements

Superconducting Quantum Interference Device (SQUID) (Quantum Design) is used to measure the room temperature magnetic properties of the FGO powders.

VI) Magnetic Resonance Imaging (MRI) phantoms

All relaxation measurements were performed using a 4.7T Biospec system (Bruker Biospin MRI, Billerica, MA) with a 30cm bore, imaging gradients with an inner diameter of 60mm, and a volume resonator with 35mm inner diameter. Serial dilutions of the contrast agent were sealed in NMR tubes and suspended in relaxed water in order to minimize the effects of susceptibility differences between the samples and their surroundings. Spin-spin (T2) relaxation times were measured using a multi-echo spin echo sequence (TEmin = 8.5ms, with 8.5ms echo spacing over 24 echoes; TR = 5000ms). All images were acquired with matching slice geometry (1mm axial sections, 32mm × 32mm field-of-view over a 64 × 64 image matrix). Relaxation time constants for each sample were measured by fitting signal decay curves to a standard model in ParaVision, the operating environment for the Biospec platform.

VII) Ultrasound and Photoacoustic phantoms

Photoacoustic and ultrasound imaging were performed using VisualSonics Vevo®LAZR-2100 high-frequency photoacoustic and VisualSonics VEVO 770 B-mode ultrasound system. In the ultrasound imaging study, acoustic coupling was achieved through ultrasound gel. Ultrasound phantom plates were scanned using a 40-MHz linear array transducer, to acquire a cross-sectional image. The gain was set to 10 decibels (dB), and all samples were scanned under the same experimental conditions. In the photoacoustic imaging study, FGO was imaged spectroscopically with a 21-MHz linear array from 680 to 970 nm to determine the peak signal produced by FGO and GO. FGO gelatin phantoms were then imaged at 720nm to acquire a cross-sectional image; acoustic coupling was achieved through a distilled water bath.

VIII) NIR laser induced photo heating

The irradiation power of the NIR laser is 1.6W, determined by a power meter (VEGA, OPHIR Japan, LTD.). *In situ* samples where exposed for 1 min to the NIR-laser and the thermal profiles were measured. The sample preparation consisted of aqueous solution of FGO (1mg mL^{-1}, 100μL) added to a confocal plate (35mm) containing DMEM (50μL). The negative control consisted of DMEM (150 μL) added into a confocal plate (35mm). To measure the thermal gradient we used a thermal imager test 881-2 (Testo AG, Germany). All the thermal data was analyzed with Testo IR software.[59]

IX) In vitro hyperthermia induced by NIR laser

Glioma (GI-1) cells ($5X10^4$ cells/well) were seeded on a confocal plate (35mm) with DMEM media and incubated overnight at 37°C and 5%CO_2. Sample preparation consisted of washing the cells with warm PBS and adding FGO (0, 400 μg mL^{-1}, 50 μL) respectively to the confocal plate that already had fresh warm DMEM (100μL). Experimental conditions were the same as the *in situ* experiment. After laser exposure, cells were washed and stained using Annexin V-FITC apoptosis detection kit and its protocol. After incubation in darkness, the cells were observed at a magnification of 20X under an inverted confocal microscope IX81 (Olympus Corp.) with a confocal scanning unit CSU-X1 (Yokogawa Electric Corp.) and coupled to an iXon DU897 CCD camera (Andor Technology) utilizing laser wavelengths of 488 and 561 nm as well as phase contrast acquisition.

Supplementary Material

Refer to Web version on PubMed Central for supplementary material.

Acknowledgments

We acknowledge Dr. Srivani Veeranarayanan, Dr. Athulya Aravind, Dr. Aby C. Polouse and Dr. M Sheikh Mohamed for the help provided in the course of this research. This work is supported by the US Army Medical Research Acquisition Act (USAMRAA), award number W81XWH-10-1-0434 and partially supported by the IMI Program of the National Science Foundation under Award No. DMR 0843934. S.A.M lab is supported by George and Barbara Bush Endowment for Innovative Cancer Research. We would also like to acknowledge Charles Kingsley and Keith A. Mitchel at the small animal ultrasound and MRI facility at MD Anderson Cancer Center, which is funded by the Cancer Center Support Grant from the National Cancer Institute (CA16672).

References

1. Ho J-AA, Wang L-S, Chuang M-C. IJN. 2012:4679. [PubMed: 22956869]
2. Xia Y, Li W, Cobley CM, Chen J, Xia X, Zhang Q, Yang M, Cho EC, Brown PK. Acc Chem Res. 2011; 44:914–924. [PubMed: 21528889]
3. Luo S, Zhang E, Su Y, Cheng T, Shi C. Biomaterials. 2011; 32:7127–7138. [PubMed: 21724249]
4. Gobin AM, Lee MH, Halas NJ, James WD, Drezek RA, West JL. Nano Lett. 2007; 7:1929–1934. [PubMed: 17550297]
5. Pissuwan D, Valenzuela SM, Cortie MB. Trends in Biotechnology. 2006; 24:62–67. [PubMed: 16380179]
6. You J, Zhang G, Li C. ACS Nano. 2010; 4:1033–1041. [PubMed: 20121065]
7. Biosciences, N. Clinical Trials gov [website on the Internet]. Bethseda: 2009.
8. Wang Y, Li Z, Hu D, Lin CT, Li J, Lin Y. J Am Chem Soc. 2010; 132:9274–9276. [PubMed: 20565095]
9. Feng L, Liu Z. Nanomedicine. 2011; 6:317–324. [PubMed: 21385134]
10. Bi S, Zhao T, Luo B. Chem Commun. 2012; 48:106–108.
11. Singh V, Joung D, Zhai L, Das S, Khondaker SI, Seal S. Progress in Materials Science. 2011; 56:1178–1271.

12. Yang K, Feng L, Shi X, Liu Z. Chem Soc Rev. 201210.1039/c2cs35342c
13. Shen H. Theranostics. 2012:283. [PubMed: 22448195]
14. Schedin F, Geim AK, Morozov SV, Hill EW, Blake P, Katsnelson MI, Novoselov KS. Nat Mater. 2007; 6:652–655. [PubMed: 17660825]
15. Gollavelli G, Ling YC. Biomaterials. 2012; 33:2532–2545. [PubMed: 22206596]
16. Liu Z. Theranostics. 2012:235. [PubMed: 22448193]
17. Katz E. ChemPhysChem. 2004
18. BAO H, PAN Y, LI L. Nano LIFE. 2012; 02:1230001.
19. Bahrami A. 2011
20. Luo X, Matranga C, Tan S, Alba N, Cui XT. Biomaterials. 2011; 32:6316–6323. [PubMed: 21636128]
21. Park S, Mohanty N, Suk JW, Nagaraja A, An J, Piner RD, Cai W, Dreyer DR, Berry V, Ruoff RS. Adv Mater. 2010; 22:1736–1740. [PubMed: 20496406]
22. Wang Y, Li Z, Wang J, Li J, Lin Y. Trends in Biotechnology. 2011; 29:205–212. [PubMed: 21397350]
23. Zhang L, Xia J, Zhao Q, Liu L, Zhang Z. Small. 2009
24. Zhang W, Guo Z, Huang D, Liu Z, Guo X, Zhong H. Biomaterials. 2011; 32:8555–8561. [PubMed: 21839507]
25. Loh KP, Bao Q, Eda G, Chhowalla M. Nature Publishing Group. 2010; 2:1015–1024.
26. Zhou L, Jiang H, Wei S, Ge X, Zhou J, Shen J. Carbon. 2012; 50:5594–5604.
27. Georgakilas V, Otyepka M, Bourlinos AB, Chandra V, Kim N, Kemp KC, Hobza P, Zboril R, Kim KS. Chem Rev. 2012:120925091858007.
28. Melancon MP, Zhou M, Li C. Acc Chem Res. 2011; 44:947–956. [PubMed: 21848277]
29. Ji X, Shao R, Elliott AM, Stafford RJ, Esparza-Coss E, Bankson JA, Liang G, Luo ZP, Park K, Markert JT, Li C. J Phys Chem C. 2007; 111:6245–6251.
30. Larson TA, Bankson J, Aaron J, Sokolov K. Nanotechnology. 2007; 18:325101.
31. Ma X, Tao H, Yang K, Feng L, Cheng L, Shi X, Li Y, Guo L, Liu Z. Nano Res. 2012; 5:199–212.
32. Narayanan TN, Gupta BK, Vithayathil SA, Aburto RR, Mani SA, Taha-Tijerina J, Xie B, Kaipparettu BA, Torti SV, Ajayan PM. Adv Mater. 2012; 24:2992–2998. [PubMed: 22573478]
33. Vermisoglou E, Pilatos G, Romanos G. 2011
34. He F, Fan J, Ma D, Zhang L, Leung C, Chan HL. Carbon. 2010; 48:3139–3144.
35. Ruiz Cabello J, Barnett BP, Bottomley PA, Bulte JWM. NMR in Biomedicine. 2011; 24:114–129. [PubMed: 20842758]
36. Díaz-López R, Tsapis N, Fattal E. Pharm Res. 2009; 27:1–16. [PubMed: 19902338]
37. Strunecka A, Patoka J, Connett P. J Appl Biomed. 2004; 2:141–150.
38. Riess J. Current Opinion in Colloid & Interface Science. 2003; 8:259–266.
39. Forsberg F, Rawool N, Merton D. Ultrasonics. 1996
40. Liu Z, Lammers T, Ehling J, Fokong S, Bornemann J, Kiessling F, Gätjens J. Biomaterials. 2011; 32:6155–6163. [PubMed: 21632103]
41. Mathkar A, Narayanan TN, Alemany LB, Cox P, Nguyen P, Gao G, Chang P, Romero-Aburto R, Mani SA, Ajayan PM. Particle Particle Systems Characterization. 2013:n/a–n/a.
42. Chantharasupawaong P, Philip R, Narayanan TN, Sudeep PM, Mathkar A, Ajayan PM, Thomas J. J Phys Chem C. 2012:121116111910007.
43. Singh SK, Singh MK, Nayak MK, Kumari S, Shrivastava S, Grácio JJA, Dash D. ACS Nano. 2011; 5:4987–4996. [PubMed: 21574593]
44. Singh SK, Singh MK, Kulkarni PP, Sonkar VK, Grácio JJA, Dash D. ACS Nano. 2012; 6:2731–2740. [PubMed: 22376049]
45. Karlicky F, Datta KKR, Otyepka M. ACS Nano. n.d
46. Duschinsky R, Pleven E. Journal of the American …. 1957
47. Marcano DC, Kosynkin DV, Berlin JM, Sinitskii A, Sun Z, Slesarev A, Alemany LB, Lu W, Tour JM. ACS Nano. 2010; 4:4806–4814. [PubMed: 20731455]

48. Gao W, Alemany LB, Ci L, Ajayan PM. Nature Publishing Group. 2009; 1:403–408.
49. Sun X, Liu Z, Welsher K, Robinson JT, Goodwin A, Zaric S, Dai H. Nano Res. 2008; 1:203–212. [PubMed: 20216934]
50. Peng J, Gao W, Gupta BK, Liu Z, Romero-Aburto R, Ge L, Song L, Alemany LB, Zhan X, Gao G, Vithayathil SA, Kaipparettu BA, Marti AA, Hayashi T, Zhu JJ, Ajayan PM. Nano Lett. 2012; 12:844–849. [PubMed: 22216895]
51. Liu Z, Robinson JT, Sun X, Dai H. J Am Chem Soc. 2008; 130:10876–10877. [PubMed: 18661992]
52. Eda G, Lin YY, Mattevi C, Yamaguchi H. Advanced …. 2010
53. Yang X, Zhang X, Liu Z, Ma Y, Huang Y, Chen Y. J Phys Chem C. 2008; 112:17554–17558.
54. Hata T, Takahashi H, Watanabe K, Takahashi M, Taguchi K, Itoh T, Todo S. Journal of the American College of Surgeons. 2004; 198:190–197. [PubMed: 14759774]
55. Tian B, Wang C, Zhang S, Feng L, Liu Z. ACS Nano. 2011; 5:7000–7009. [PubMed: 21815655]
56. Yang K, Zhang S, Zhang G, Sun X, Lee ST, Liu Z. Nano Lett. 2010; 10:3318–3323. [PubMed: 20684528]
57. Robinson JT, Tabakman SM, Liang Y, Wang H, Sanchez Casalongue H, Vinh D, Dai H. J Am Chem Soc. 2011; 133:6825–6831. [PubMed: 21476500]
58. Moros, E. Physics of Thermal Therapy. CRC Press; 2012.
59. TAG. 0981 7374/dk/Si/Q/08.2009. 2009:1–14.

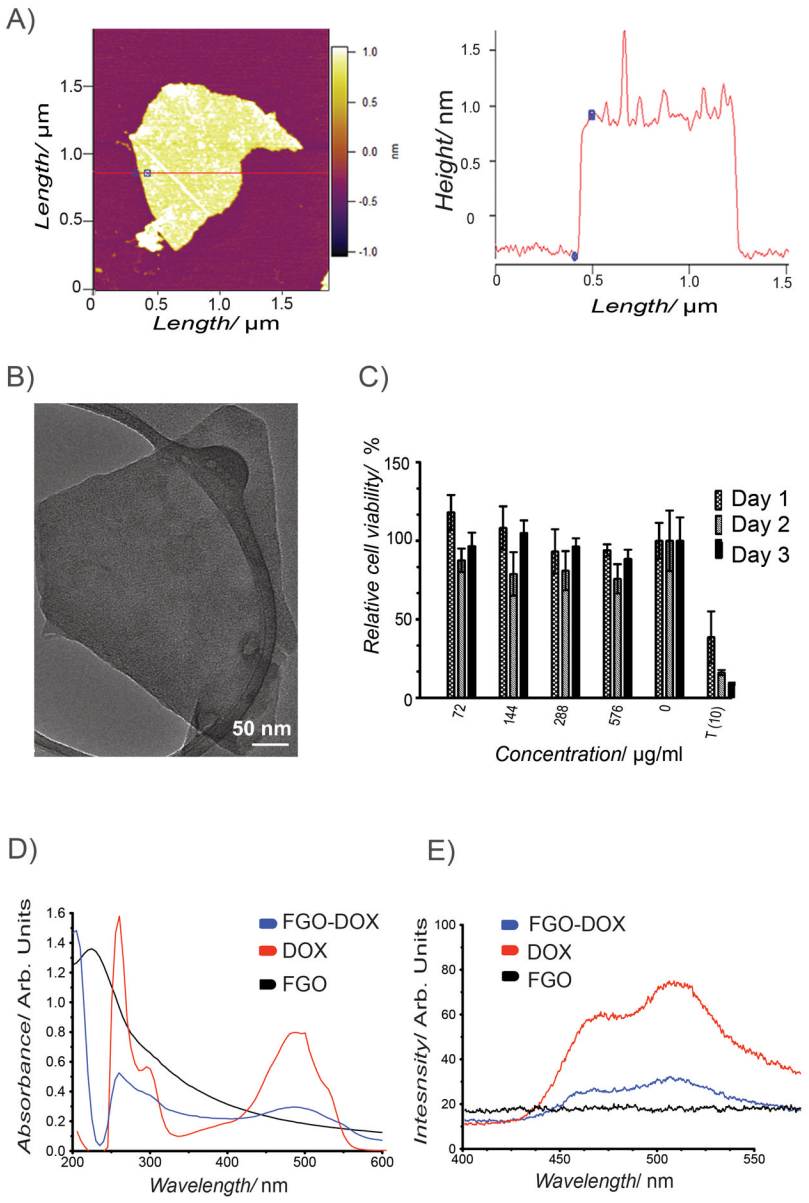

Figure 1.

FGO Characterization. (A) AFM analysis of FGO including height profile. (B) TEM image of FGO. (C) Concentration and time dependent MTT assay to determine cell viability after incubation with FGO, T(10) is the positive control (taxol 10 μg mL^{-1}). Bars denote mean standard deviation error. (D) Absorption spectra of FGO-DOX (blue), DOX (red) and FGO (black). (E) Photoluminescence spectra of FGO-DOX (blue), DOX (red), FGO (black).

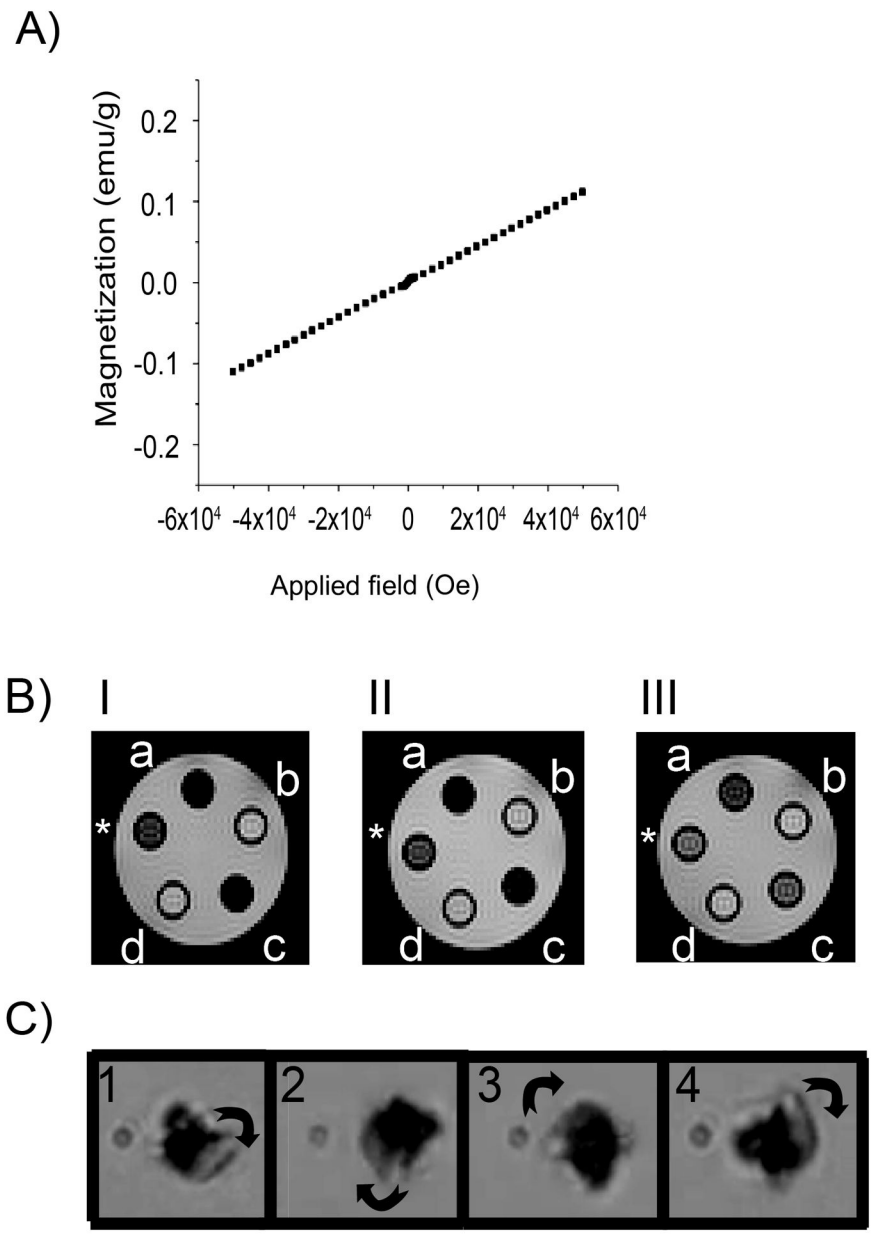

Figure 2.

Magnetic properties of FGO. (A) SQUID magnetization curve. (B) Spin-spin (T2) relaxation measurements acquired on a 4.7T MRI of FGO (I a= 625, c= 500; II a=313, c= 250; III a=156, c=125μg mL^{-1}) and GO (I b= 625, d= 500; II b=313, d= 250; III b=156, d=125μg mL^{-1}). The positive control (*) consists of diluted magnevist (0.5mg mL^{-1}). (C) Rotational magnetic field snapshots of FGO under a field of 12mT, rotation is clockwise.

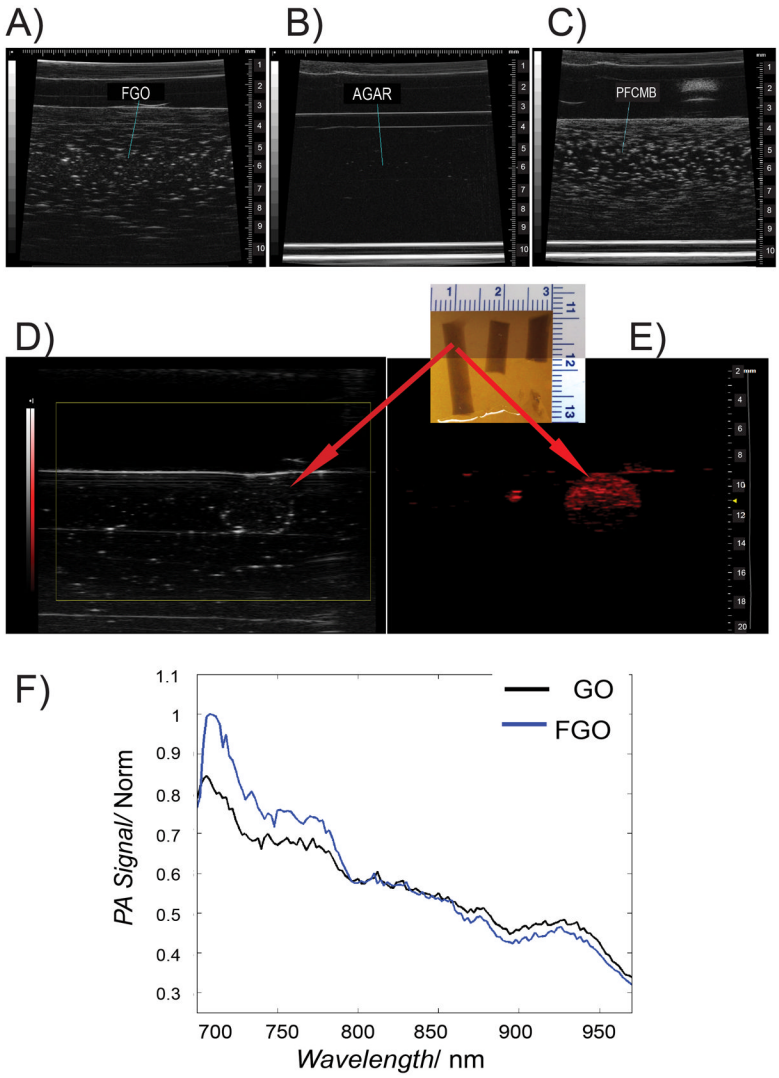

Figure 3.

Ultrasound and photoacoustic behavior of FGO. (A) Ultrasound imaging of FGO, (B) Agar and (C) perfluorocarbon microbubbles (PFCMB) in a 40MHz linear array transducer. (D and E) Photoacoustic FGO gelatin phantom under a 21MHz ultrasound equipment coupled with a VisualSonics Vevo LAZR system at 720nm. (F) Photoacoustic normalized signal spectrum of FGO (blue) and GO (black).

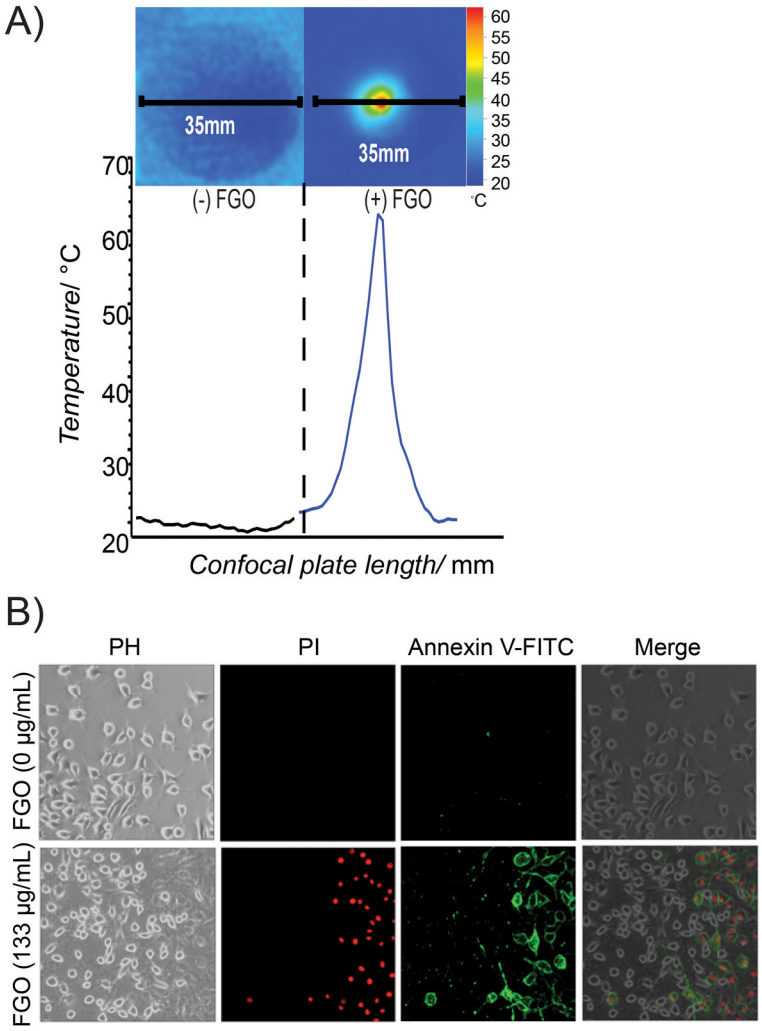

Figure 4.

Hyperthermia cell ablation facilitated by FGO. (A) NIR-laser-induced hyperthermia of DMEM medium (-) FGO and of (+) FGO. Each confocal plate length is 35mm. (B) *In vitro* NIR-laser induced differential photothermal ablation of glioma cells (GI-1) incubated with 0μg mL^{-1} of FGO (top) or 133μg mL^{-1} of FGO (bottom) using an apoptotic/necrotic staining and observed by optical microscopy.